CALCULATION OF HYDROGEN BETA COLOR INDICES FOR DELTA SCUTI STARS

by

Debora Kay Merrell

A senior thesis submitted to the faculty of

Brigham Young University

in partial fulfillment of the requirements for the degree of

Bachelor of Science

Department of Physics and Astronomy

Brigham Young University

August 2009

BRIGHAM YOUNG UNIVERSITY

DEPARTMENT APPROVAL

of a senior thesis submitted by

Debora Kay Merrell

This thesis has been reviewed by the research advisor, research coordinator, and department chair and has been found to be satisfactory.

Date	Eric Hintz, Advisor
Date	Eric Hintz, Research Coordinator
Date	Ross Spencer, Department Chair

ABSTRACT

CALCULATION OF HYDROGEN BETA COLOR INDICES FOR DELTA SCUTI STARS

Debora Kay Merrell

Department of Physics and Astronomy

Senior Thesis

In order to complete the Rodriguez et al. (2000) table of Hydrogen β (Hβ) color indices of δ Scuti stars, 167 δ Scutis north of -01 degrees declanation and brighter than 13th magnitude were spectroscopically observed. An improved method of reduction techniques is used on stars all the stars observed with previously unpublished Hβ color indices.The Hβ color indices of 22 δ Scuti stars are calculated.

ACKNOWLEDGMENTS

First, thank you to my fiance Bryson for reading this thesis over and over and always being a great support. I love you so much. Thank you to my advisor, Dr. Hintz, for all the guidance he provided with this research and the advice he provided on the structure of this paper. I have learned a lot over the past four years and have grown to truly love astronomy. And thank you to my parents, Debbie and Steve, my sister Jackie, and my brothers Stephen and Sam for always believing in and supporting me.

Contents

List of Tables

List of Figures

Chapter 1

Introduction and Background

1.1 Project Motivation

A star's lifetime is too long for stellar evolution to be observed in its entirety from one star. We must instead collect snapshots of numerous stars which are at different points in their lifetime and piece the puzzle together. Characteristics such as temperature, distance, motion, position, rotation, and size are all important to gain an understanding of the structure and evolution of a star. The collection of light from stars is the only way for stellar objects to be studied; therefore astronomers use unique techniques, specialized for each desired characteristic, to collect this light. Spectroscopy is one of these light collection techniques. In spectroscopy, light collected from the stellar source is split into a wide range of wavelengths so that the star can be analyzed at many wavelengths.

The Brigham Young University Astronomy Research Group has been involved in the study of δ Scuti stars for many years. The most complete catalog of δ Scuti stars and their characteristics was compiled by Rodriguez et al. (2000) and includes a list of the known δ Scutis along with each star's pulsation period and pulsation amplitude. The list also includes the rotational velocities, radial velocities, spectral type, and different color index values. There are 636 δ Scutis stars listed in this catalog. Of these, 417 of the stars are brighter than 13th magnitude. Only 339 or 53% of the stars listed have a Hydrogen β (Hβ). Of the stars brighter than 13th magnitude about 20% of the stars do not have a listed Hβ color index. The data used in this research has been previously analyzed by Tabitha Bush in a masters thesis, however the Hβ color indices were only found for 5 δ Scuti stars. This thesis is an expansion and improvement on that work.

1.2 Delta Scuti Stars

Variable stars are stars whose light output changes periodically over a specific time frame. The two main groups of variable stars include: extrinsic and intrinsic variables. Extrinsic variables are those that seem to be varying due to the star's relative position to the Earth. An example of an extrinsic variable would be an eclipsing binary system. The light output of the system fluctuates as one star eclipses the other. An intrinsic variable is one that varies due to a physical process occurring on the star, such as an eruption on the star or a pulsation of size or temperature of the star. δ Scuti stars are intrinsic variables which pulsate at periods ranging from 20 minutes to five hours.

Variable stars are in an instable phase of their stellar evolution. A graphical representation of stellar evolution is shown in a Hertzsprung-Russell (H-R) diagram as shown in Figure 1.1. The H-R diagram is a plot of temperature vs. stellar luminosity. The x axis is traditionally expressed as temperature, spectral type, or color and is inverted. The y axis is either stellar luminosity or absolute magnitude (both a measure of brightness), and is also inverted. The spectral type of a star is a classification that includes seven main classifications each with 10 subclasses. Table 1.1 is a list of spectral types and their corresponding temperatures. The youngest and hottest stars are O type, and the oldest and coolest stars are type M. δ Scuti stars range in spectral type from A0 to F5.

As large numbers of stars are plotted on the H-R diagram, patterns emerge. These patterns indicate different stages in a star's lifetime. The most prominent trend runs through the middle of the plot from the upper left corner to the lower right, and is called the Hydrogen Main Sequence. Stars on the Hydrogen Main Sequence are in the middle of their lifetime. They are stable stars fusing hydrogen into helium inside their cores. These stars are in a state of hydrostatic equilibrium, where the outward pressure from the fusion balances the inward pull of gravity. Our Sun is on the Hydrogen Main Sequence. Other trends in the H-R diagram include the Red

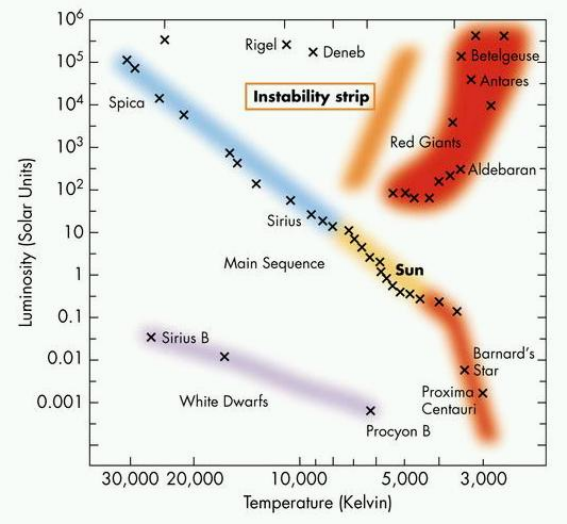

Figure 1.1: Hertzsprung-Russell diagram. Image from www.astro.umass.edu

Table 1.1. Stellar Spectral Types

Spectral Type	Color	Surface Temp. (K)
O	Blue	30,000 to 60,000
B	Blue-White	10,000 to 30,000
A	White	7,500 to 10,000
F	Yellow-White	6,000 to 7,500
G	Yellow	5,000 to 6,000
K	Yellow-Orange	3,500 to 5,000
M	Red	under 3,500

Giants and the White Dwarfs. These are stars at the end of their lifetime that have fused all of their hydrogen and are beginning to slowly die. Another trend in the H-R diagram, as shown in Figure 1.1, is the instability strip. This is the region in which variable stars are located. δ Scuti stars are located just above the main sequence, and are therefore recently out of the hydrogen fusion section of their lives.

1.3 Spectroscopy

In order to analyze a star, one must study its light output. Light exhibits both particle and wave-like properties but for this application its wave-like property

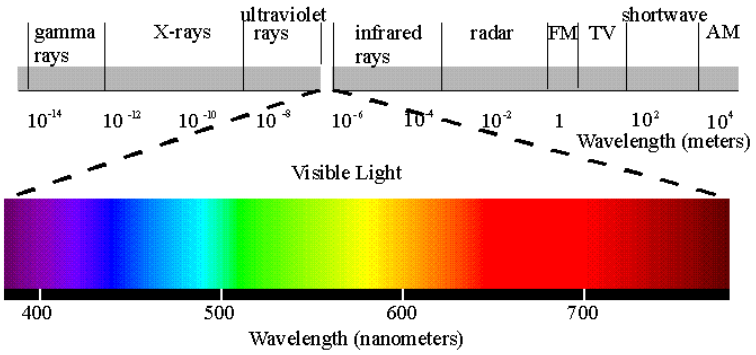

Figure 1.2: Electromagnetic spectrum. Image from dnr.sc.gov

will be most relevant. Just as waves on the sea, light waves have periodic peaks. The distance from one peak to the next is the wavelength of the light. We see light of different wavelengths as different colors. Figure 1.2 shows the entire electromagnetic spectrum. Visible light only makes up a small portion of the scale. White light is a compilation of all visible wavelengths. The electromagnetic spectrum was first discovered in 1666 by Isaac Newton when he split white light into a spectrum with a prism. Dark lines at certain wavelengths were later discovered within some spectra (referred to as absorption spectra) and connected to different elements. All matter is made of atoms and these atoms contain certain energy shells that their electrons reside in. In order for an electron to move to a shell of higher energy it must absorb a particle of light, called a photon, which has the same energy as the difference between the atom's two energy shells. Because these photons at a specific wavelength are absorbed by the atom, there appears a dark line on the spectra.

Spectroscopy is the study of light that has been dispersed into a range of wavelengths. Absorption spectra are the kind of spectra collected from stellar objects and are the kind studied in this project. A spectrograph is the device used to collect these spectra. A diagram of a simple spectrograph is shown in Figure 1.3. Light collected from a telescope is directed into a spectrograph and focused through a

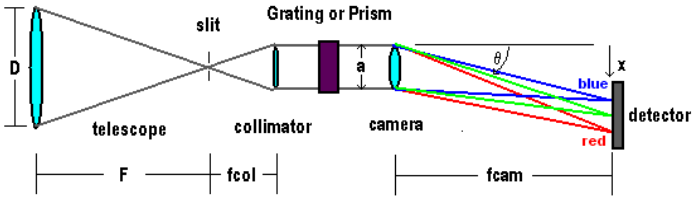

Figure 1.3: Basic spectrograph. Image from www.astro.ufl.edu

small slit opening. The light then passes through a collimating lens which makes the rays all parallel. Those parallel rays then hit a diffraction grating or prism which disperses the light into its component wavelengths. A diffraction grating is a glass piece with fine parallel grooves cut into it. These grooves can be cut in such a way to focus the diffracted light mostly of a specific order and wavelength. This process is called grazing the diffraction grating. (Richardson (1968))

The dispersed light is then recorded with some detection device. The device used in this study is a charged-coupled device, or CCD. A CCD is the same device used in most digital camera to record a picture. In this case, the CCD records the stellar spectra being collected. A CCD chip is an array of pixels that act as wells for the incoming light. When photons hit the CCD surface it triggers electrons to collect in each pixel well. The number of electrons in the well can be counted to determine the magnitude of the incoming light. Two examples of stellar spectra detected by a CCD are shown in Figure 1.4.

1.4 Hydrogen-Beta Color Index

A black body is an object that absorbs all electromagnetic radiation. A cold object would be black but a hot black body emits light that is dependent on the temperature of the object. Max Planck modeled how the intensity of electromagnetic radiation emitted by a black body is dependent on the frequency (color) and the temperature of the object. This relation is shown in Figure 1.5. A star can essentially be treated as a black body emitter. As evident in the Planck curve (Figure 1.5), a

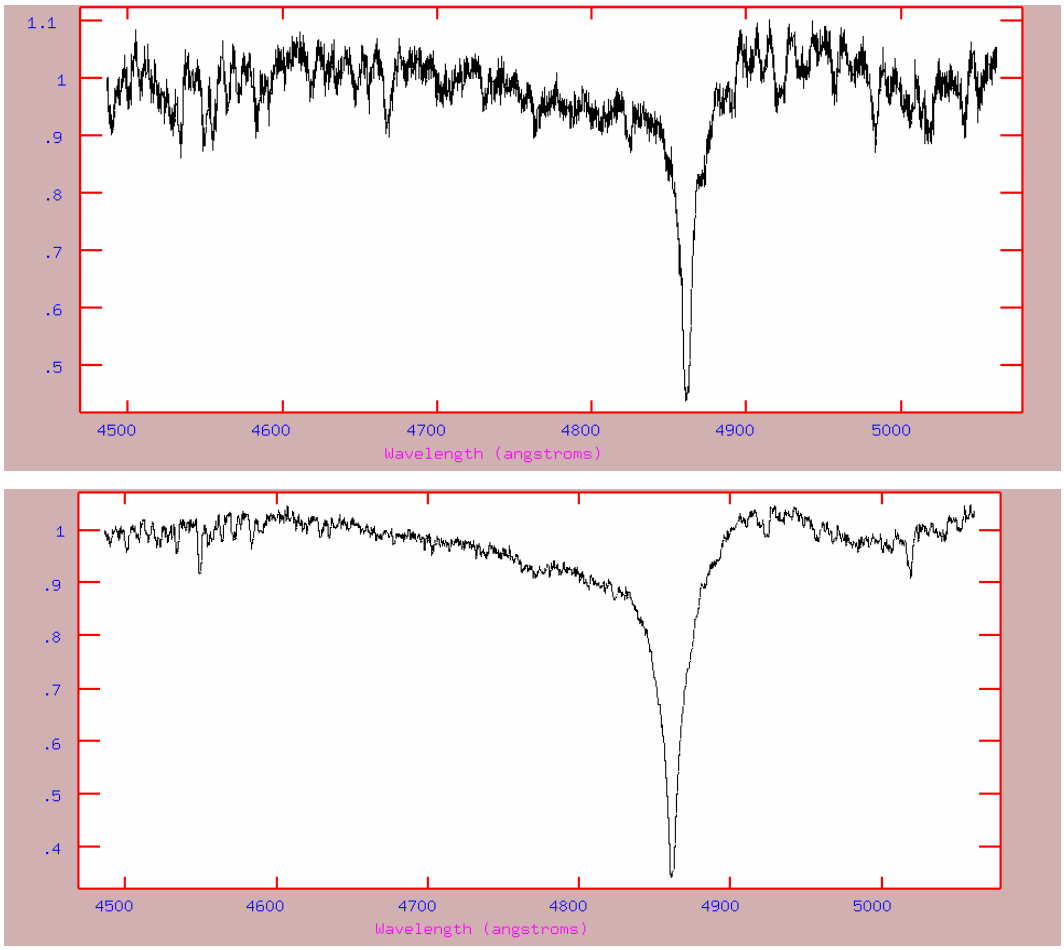

Figure 1.4: A spectrum of HQ Ursae Majoris obtained on 3 Mar 2002 (*top*). A spectrum of HD 120500 obtained on 3 March 2002 (*bottom*).

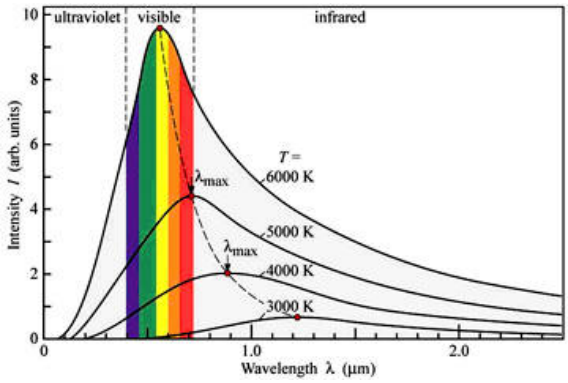

Figure 1.5: Planck curves. Image from www4.nau.edu

blue star is hotter, while a red star is cooler. A star of different temperature would have a different Planck cure, therefore a star's temperature can be determined by its color index. The color index of a star is the difference between its magnitudes at different wavelengths. Equation 1.1 describes the color index where m is the star's magnitude at the wavelength, λ.

$$CI = m(\lambda_1) - m(\lambda_2) \tag{1.1}$$

The longer wavelength magnitude is subtracted from the shorter wavelength magnitude. A common photometric color magnitude is the (B-V). This is the magnitude of a star in the blue wavelength region minus the magnitude of the visual wavelength range. Color indices are instrument dependent therefore they are calibrated in such a way that the (B-V) color index of a star with the temperature of 10,000 K is zero. Thus the smaller the color index the bluer or hotter an object is, and the higher the index the cooler and more red an object. A very hot blue star will have a negative color index while a cool red star will have a positive index.

A Hydrogen β color index is similar to the photometric (B-V) color index but the index is determined by the magnitude difference found through the use of a narrow and wide filter center on a single wavelength. In this case the line is the Hydrogen

β line located at 4861 Å . This color index is a much more accurate measurement of a star's temperature because it is free of reddening affects. Interstellar dust scatters light at different wavelengths unevenly. Blue light is scattered more than red light. If the index is centered on one wavelength then the reddening will be the same for both magnitudes. Crawford & Mander (1966) discusses the standardization of 80 stars for the Hβ system. In order to obtain the magnitude measurements, two filters were used. A narrow filter with a full width half max (FWHM) of approximately 30 Å , and a wide filter with a FWHM of 150 Å . The color index of the star is found through Equation 1.2,where $F(\beta_W)$ is the flux of the star through the wide filter, and $F(\beta_N)$ is the flux of the star through the narrow filter. (Zeilik & Gregory (1998))

$$H\beta = -2.5 \log \left[F(\beta_W)/F(\beta_N)\right] \tag{1.2}$$

Equation 1.3 shows this relation in magnitudes.

$$H\beta = m(\beta_N) - m(\beta_W) \tag{1.3}$$

The flux through the two filters is determined by the transmission curves of the narrow and wide filters. Figure 1.6 shows the transmission curves used by Crawford & Mander (1966). The amount of light that passes through each filter is determined by these transmission curves and with those fluxes the Hβ color index is found.

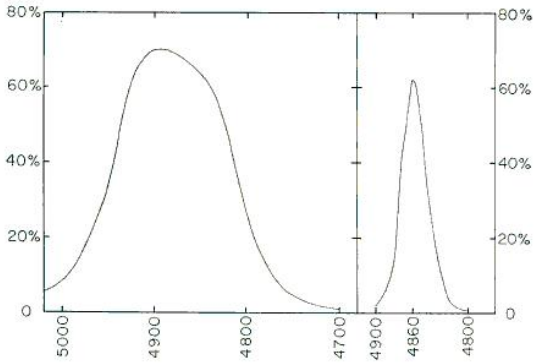

Figure 1.6: Transmission curves for Hβ filters Crawford & Mander (1966).

Chapter 2

Observations

2.1 Data Collection

The Rodriguez et al. (2000) catalog of δ Scuti stars contains 636 stars. Of those 636 stars, 339 of them do not have a published Hydrogen β color index. Spectroscopic observations, centered on the Hydrogen β region, were taken over the course of eight nights in 2002 and 2003 from the Dominion Astrophysical Observatory near Victoria, Canada. Approximately 1200 object frames were taken of δ Scuti stars on the Rodriguez et al. (2000) catalog brighter than 13th magnitude. Stars brighter than 13th magnitude were chosen because of the limitations of the equipment. The stars observed were taken from the Rodriguez et al. (2000) catalog and the values published in that paper were used as calibrating stars for each night. Tables 2.1 through 2.4 show the observed stars, broken down into magnitude ranges.

Typically 10-15 flat frames were taken per night and approximately 15-20 bias frames. Arc frames were taken in such a way that there would be an arc taken before an object and one after. This sandwiching of arc frames is done so that the telescope has the same position and orientation on the arc frame as it did with the object. This technique helps reduce the effects instrumentation orientation has on the frames.

2.2 Equipment

2.2.1 Dominion Astrophysical Observatory

The Dominion Astrophysical Observatory (DAO) is located in Saanich near Victoria, Canada. The observatory is the largest observatory in Canada and is used by many astronomers to collect both photometric and spectroscopic observations. The observatory currently houses two telescopes: the 1.2 meter McKellar Telescope and

Table 2.1. Spectroscopic Observations of δ Scutis Brighter Than 7th Magnitude

Star	V mag	Observing Run	# Obs.	Star	V mag	Observing Run	# Obs.
41 Peg	6.33	Aug 2002	3	V340 And	5.55	Aug 2002	3
AI CVn	6.03	Mar 2002	25	V352 Aur	6.16	Feb 2003	2
AO CVn	4.72	Jun 2002	3	V376 Per	5.95	Feb 2003	3
AZ CMi	6.46	Feb 2003	4	V377 Cep	6.61	Aug 2002	2
BT Cnc	6.65	Feb 2003	2	V386 Per	6.54	Feb 2003	3
CL Dra	4.96	Jun 2002	4	V388 Cep	5.56	Aug 2002	2
CN Boo	5.98	Jun 2002	2	V480 Tau	5.08	Feb 2003	2
CN Dra	6.34	Jun/Aug 2002	6	V483 Tau	5.58	Feb 2003	3
CO Lyn	6.83	Mar 2002	5	V509 Per	6.48	Feb 2003	3
CX Cnc	6.05	Feb 2003	3	V521 Per	6.38	Feb 2003	3
CX UMa	6.93	Mar 2002/Feb 2003	2	V526 Cas	6.38	Aug 2002	5
DD UMa	4.80	Feb 2003	3	V620 Her	6.20	Jun/Aug 2002	5
DK Vir	6.69	Jun 2002	1	V644 Her	6.35	Jun 2002	4
DP UMa	5.22	Jun 2002	4	V696 Tau	5.26	Feb 2003	1
EM Aqr	6.55	Aug 2002	3	V775 Tau	5.72	Feb 2003	3
EN UMa	5.88	Mar 2002	2	V777 Tau	4.48	Feb 2003	3
EP Cnc	6.77	Feb 2003	3	V784 Cas	6.66	Feb 2003	3
ER Dra	6.26	Jun 2002	1	V831 Her	6.34	Jun/Aug 2002	6
FI UMa	6.63	Feb 2003	4	V1004 Ori	5.89	Feb 2003	3
FM Com	6.46	Jun 2002	3	V1208 Aql	5.53	Jun/Aug 2002	6
FM Vir	5.22	Jun 2002	3	V1276 Cyg	6.54	Jun/Aug 2002	5
FP Ser	6.28	Mar 2002	3	V1431 Aql	5.79	Jun 2002	2
FQ Boo	6.60	Mar 2002	3	V1644 Cyg	4.93	Jun/Aug 2002	19
GG Vir	6.22	Jun 2002	2	V2112 Oph	6.51	Jun/Aug 2002	6
GN And	5.20	Aug 2002	3	VV Ari	6.70	Aug 2002	2
GX Peg	6.33	Aug 2002	5	VW Ari	6.70	Aug 2002	5
HT Peg	5.30	Aug 2002	7	VX Psc	6.01	Aug 2002	6
II Vir	6.52	Mar 2002	1	VY Psc	6.55	Aug 2002	3
IK Peg	6.08	Aug 2002	3	XX Psc	6.11	Aug 2002	3
IM Tau	5.39	Feb 2003	3	β Cas	2.28	Aug 2002	3
IQ Vir	6.31	Jun 2002	3	β Vir	3.61	Mar 2002	4
KW 284	6.76	Feb 2003	3	γ Boo	3.04	Jun 2002	3
KW Aur	5.01	Mar 2002	3	δ Del	4.43	Aug 2002	3
LT Vul	6.61	Jun/Aug 2002	6	δ Ser	3.80	Aug 2002	2
NU Vul	5.19	Jun/Aug 2002	6	ϵ Cep	4.18	Aug 2002	3
OX Aur	6.10	Feb 2003	2	θ2 Tau	3.40	Feb 2003	3
RX Sex	6.68	Mar 2002	2	ι Boo	4.75	Jun 2002	3
SAO 52892	6.51	Aug 2002	3	κ2 Boo	4.53	Mar 2002	3
SAO 72399	6.54	Aug 2002	3	λ Boo	4.18	Jun 2002	3
SAO 88295	5.51	Aug 2002	2	ν UMa	3.78	Feb 2003	6
SAO 141427	6.25	Jun 2002	4	ρ Tau	4.65	Feb 2003	3
SAO 143373	6.50	Aug 2002	4	τ Peg	4.58	Aug 2002	2
UU Ari	6.14	Feb 2003	2	υ Tau	4.28	Feb 2003	3
UV Ari	5.17	Feb 2003	3				

Table 2.2. Spectroscopic Observations of δ Scutis from 7th to 8th Magnitude

Star	V Mag	Observing Run	# Obs.	Star	V Mag	Observing Run	# Obs.
AD Ari	7.43	Aug 2002	3	V1745 Cyg	7.44	Jun 2002	3
AR Ari	7.82	Feb 2003	2	V2084 Cyg	7.35	Jun 2002	3
BH Psc	7.12	Aug 2002	3	V2109 Cyg	7.51	Jun 2002	3
BN Cnc	7.8	Feb 2003	2	V2109 Cyg	7.51	Aug 2002	21
BU Cnc	7.67	Feb 2003	3	V2314 Oph	7.43	Jun 2002	3
BX Cnc	7.96	Feb 2003	3	V2314 Oph	7.43	Aug 2002	3
BY Cnc	7.9	Feb 2003	3	V345 Gem	7.78	Mar 2002	3
CQ Lyn	7.97	Feb 2002	35	V350 Peg	7.2	Aug 2002	3
		Mar 2003	4			Sep 2003	6
CR Lyn	7.65	Mar 2002	5	V361 And	7.71	Aug 2002	3
DL UMa	7.2	Mar 2002	3	V365 And	7.42	Aug 2002	3
DQ Cep	7.26	Jun 2002	2	V373 And	7.58	Aug 2002	3
		Aug 2002	2	V377 Cas	7.83	Aug 2002	2
DR Psc	7.23	Aug 2002	3			Sep 2003	3
DX Cet	7	Aug 2002	2	V383 Vul	7.17	Jun 2002	4
EE Cam	7.71	Mar 2002	4			Aug 2002	3
EO UMa	7.12	Mar 2002	3	V396 And	7.86	Aug 2002	3
		Feb 2003	35	V456 Aur	7.83	Mar 2002	7
FL Cnc	7.03	Mar 2002	3	V459 Cep	7.65	Aug 2002	3
HIP 59015	7.54	Mar 2002	6	V479 Tau	7.44	Feb 2003	3
		Feb 2003	17	V544 Lyr	7.45	Jun 2002	3
HQ UMa	7.11	Mar 2002	3			Sep 2003	3
IP UMa	7.66	Jun 2002	4	V579 Per	7.84	Feb 2003	3
		Feb 2003	32	V650 Tau	7.76	Feb 2003	3
KW 385	7.92	Feb 2003	4	V764 Mon	7.16	Mar 2002	3
NN Peg	7.25	Aug 2002	3	V929 Her	7.99	Jun 2002	3
NT Hya	7.37	Mar 2002	6	V966 Her	7.98	Mar 2002	3
PV Gem	7.52	Mar 2002	3			Aug 2002	2
SAO 16394	7.53	Jun 2002	3			Feb 2003	18
SAO 43050	7.79	Feb 2003	3			Sep 2003	6
SAO 74848	7.89	Aug 2002	4	VZ Cnc	7.73	Mar 2002	10
SAO 107656	7.56	Aug 2002	3				
SAO 140074	7.84	Jun 2002	2				
V1438 Aql	7.72	Jun 2002	2				
		Aug 2002	9				
		Sep 2003	1				

Table 2.3. Spectroscopic Observations of δ Scutis from 8th to 9th Magnitude

Star	V Mag	Observing Run	# Obs.
EI Dra	8.54	Jun 2002	3
GG UMa	8.66	Mar 2002	3
GS UMa	8.68	Mar 2002	1
IN Dra	8.02	Aug 2002	3
QS Gem	8.84	Mar 2002	3
SAO 22973	8.56	Feb 2003	3
SAO 43060	8.14	Feb 2003	2
SAO 55300	8.78	Aug 2002	1
SAO 75119	8.25	Aug 2002	2
TU UMi	8.77	Jun 2002	2
V360 Cep	8.52	Aug 2002	3
V549 Lyr	8.06	Jun 2002	3
		Sep 2003	3
V873 Her	8.39	Jun 2002	3
		Feb 2003	12
		Sep 2003	2
V919 Her	8.36	Jun 2002	3
V979 Her	8.48	Jun 2002	3
V1719 Cyg	8.01	Aug 2002	19
V2129 Cyg	8.32	Aug 2002	2
V2088 Cyg	8.24	Jun 2002	2

Table 2.4. Spectroscopic Observations of δ Scutis from 9th to 13th Magnitude

Star	V Mag	Observing Run	# Obs.
GW Dra	9.31	Mar 2002	6
		Feb 2003	4
GW UMa	9.6	Mar 2002	2
		Feb 2003	6
V1003 Her	9.76	Aug 2002	1
		Feb 2003	2
V336 Sge	9.3	Aug 2002	1
V830 Her	9.3	Jun 2002	2
AN Lyn	10.66	Feb 2003	6
V577 Oph	10.8	Feb 2003	3
V927 Her	10.08	Feb 2003	6
CW Ser	11.98	Feb 2003	6
V567 Oph	11.08	Feb 2003	4
V959 Oph	11.4	Feb 2003	2
BO Lyn	12	Feb 2003	12

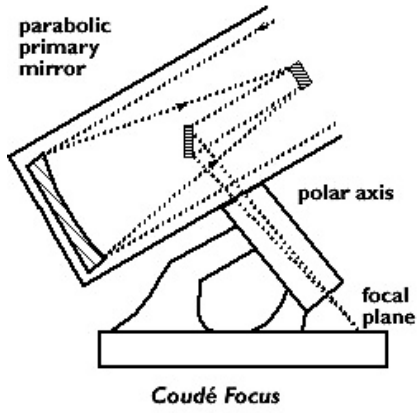

Figure 2.1: Coudé telescope focus. Image from www.as.utexas.edu

the 1.8 meter Plaskett Telescope. The Plaskett Telescope was the original telescope of the observatory. The 1.2 meter McKellar telescope is equiped with a spectrograph. Objects examined for this research project were obtained via the spectrograph of the 1.2 meter telescope.

The observatory is located in a good location to take specrtroscopic observations. It is in a remote location that reduces light pollution. The location also provides good seeing conditions.

2.2.2 Telescope and Spectrograph

The 1.2 m McKellar Telescope was used to secure spectra for 167 of the 233 northern hemisphere δ Scuti stars brighter than 13th magnitude. The 1.2 m telescope is a reflection telescope with a Coudé focus. The Coudé focus uses three mirrors to direct the light down the polar axis of the telescope. Figure 2.1 shows the configuration of a Coudé focus telescope. The light from the telescope is then funneled into the slit opening of the spectrograph. The spectrograph grating is a 32121 grating blazed at 5000 Å and yields a 10.1 Å/mm. Table 2.5 lists the central wavelength and coverage of the reflection grating.

Table 2.5. Spectrograph Specifics

Observing Run	Central Wavelength (Å)	Coverage (Å)
March 2002	4825	4500 to 5150
June 2002	4700	4400 to 5000
August 2002	4700	4400 to 5000
February 2003	4800	4400 to 5000

Table 2.6. CCD Specifics

Observing Run	Plate Scale (Å/Pixel)
March 2002	0.163
June 2002	0.150
August 2002	0.150
February 2003	0.175

2.2.3 Charged Coupled Device

The Charged Coupled Device, or CCD, is the most commonly used detector today due to its high quantum efficiency compared to other detectors. The quantum effiicency of modern CCD's can reach up to 60%. The CCD used for this project was the SITe4 CCD used on the spectrograph. The dimentions of the CCD were pixels, with a pixel size of 15 micron pixels. Table 2.6 contains a list of the plate scale of the CCD used for each observing run.

Chapter 3

Data Reduction

3.1 Image Reductions

All 167 δ Scuti stars observed were reduced using the standard spectral reductions package in the Image Reduction and Analysis Facility (IRAF). Calibration frames, such as flat and bias frames, are applied to the raw image frames in order to remove features that are not caused by the observed object. Features caused by the uneven response of the CCD pixels, or the electronics of the equipment are examples of features that calibration frames remove. Arcs are also a form of calibration frames that are used to wavelength calibrate the object frames. This converts the x-axis of the object frames from pixels to wavelength (Å). Figure 3.1 shows examples of calibration frames and an unprocessed image frame. Once the raw object frames have been reduced they are then suitable to analyze. More detail of the reduction process is given in the following sections.

3.1.1 Updating Headers and Trimming Frames

Image headers contain basic information that may be needed for the reduction process. Each different reduction package needs different material in the file headers so the headers must be updated for the specific purpose. Some examples of standard information contained within a header are image name, filter(s) used, exposure time, observation date and time. The headers are a good way to keep track of what has been done to the frame as any processing that has been done on the frame will appear in the header with a date and time of processing. Figure 3.2 is an example of a image header taken from the star τ Pegasi. This image has been processed as evident from the information at the bottom of the header.

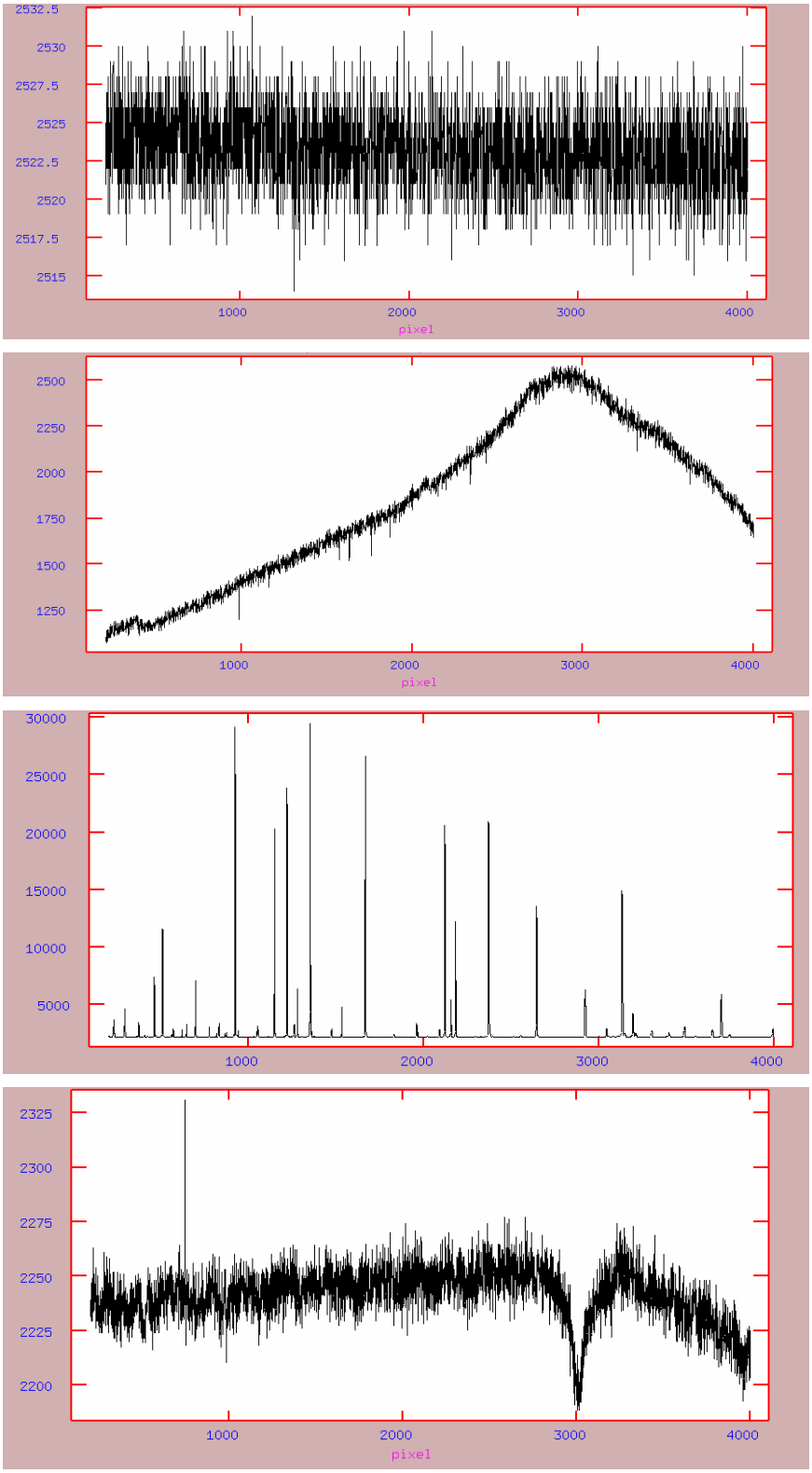

Figure 3.1: Unprocessed bias frame (*top*), flat field frame (*second*), FeAr arc frame (*third*), and object frame (XX Piscium) (*bottom*).

```
taupegcr0001.imh[360,3991][real]: tau Peg
No bad pixels, min=unknown, max=unknown
Line storage mode, physdim [384,3991], length of user area 1904 s.u.
Created Tue 00:11:12 27-Mar-2007, Last modified Tue 00:11:16 27-Mar-2007
Pixel file "romana!/home/iraf/images/tabitha/taupegcr0001.pix" [ok]
'DAO'                   /
New copy of taupeg0001.imh
New copy of taupeg0001.imh
New copy of taupeg0001.imh
EXPTIME =                  200 /
INSTRUME= 'SITe-4'             /
XBIN    =                    1 /
YBIN    =                    1 /
PIXSIZE =                   15 / pixel size, microns
CTYPE1  = 'PIXEL   '           /15 / axis1 in pixels
CTYPE2  = 'PIXEL   '           /15 / axis2 in pixels
CCDTEM  =                -59.0 /
DATE-OBS= '2002-08-11T09:59:17'/
RA      = '23:21:03.52'         /  AT START OF EXPOSURE
DEC     = '23:46:24.90'         /  AT START OF EXPOSURE
EPOCH   = '2002.63             ' / OF RA and DEC AT START OF EXPOSURE
SIDEREAL= '23:04:27.72         ' / AT START OF EXPOSURE
HA      = '-00:16:36.80        ' / AT START OF EXPOSURE
OBSTYPE = 'object              ' / OBSERVATION TYPE
OBSERVER= 'Hintz'
IMAGETYP= 'object  '
DISPAXIS= '2       '
RDNOISE = '7       '
GAIN    = '1.8     '
OBSERVAT= 'dao     '
OBS     = '@observat'
ST      =    23.0743666666667
AIRMASS =             1.102531
UTMIDDLE= '10:01:40.0'
JD      =    2452497.91732639
HJD     =    2452497.92121065
LJD     =             2452497.
WCSDIM  =                    2
CDELT1  =                   1.
CDELT2  =                   1.
CD1_1   =                   1.
CD2_2   =                   1.
LTM1_1  =                   1.
LTM2_2  =                   1.
WAT0_001= 'system=image'
WAT1_001= 'label=pixel'
WAT2_001= 'label=pixel'
TRIM    = 'Mar 26 23:56 Trim data section is [1:360,10:4000]'
CCDSEC  = '[1:360,10:4000]'
CRPIX2  =                  -9.
LTV2    =                  -9.
CCDPROC = 'Mar 27  0:04 CCD processing done'
ZEROCOR = 'Mar 27  0:04 Zero level correction image is Zero.imh'
FLATCOR = 'Mar 27  0:04 Flat field image is nFlat.imh with scale=1.'
CRCOR   = 'Threshold= 25.0, fluxratio=  2.00, removed=1359'
REFSPEC1= 'arc0020 '
```

Figure 3.2: Example of image header file for τ Pegasi.

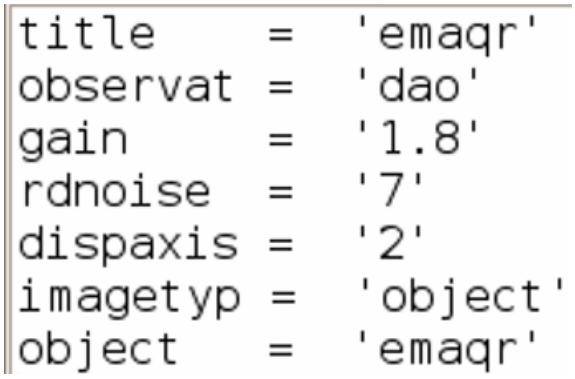

Figure 3.3: Example of *.cmds* file for EM Aquarii.

Information can be added to the header using a *.cmds* file. An example of a *.cmds* file used in this study is shown in Figure 3.3. After the *.cmds* file updates the frame header the airmass and the Heliocentric Julian Date (HJD) must be added to the header. The airmass is a measure of the amount of atmosphere the light from a star must travel through to reach the telescope. At the zenith (90 degrees from the horizon) the airmass is defined to be 1, and 30 degrees above the horizon the airmass is said to be 2. A relation is used to determine the airmass of all points in between. The HJD is simply a way for astronomers to keep track of time without the effects of Earth's orbit. Light coming from a star will take a different amount of time to reach the Earth when the Earth is at different locations in it's orbit. The HJD takes into account this time difference.

The pixels on the outer edge of CCD chips usually do not have the same response as the center ones of contain columns of bad pixels. The SITe4 CCD used in this study contains bad columns on the edge of the chip. Fortunately, the data on the edge of the chip is not necessary for reduction or analysis so all frames are trimmed using the IRAF command *ccdproc*. For this study 200 pixel columns were trimmed off from each side of the frame.

3.1.2 Processing Bias Frames

After the image headers have been updated, the calibration frames are processed and applied to the image frames. A bias frame is a calibration frame used to account for electrons coming from the telescope and detection device system and not the star's light. The frame is taken with a zero-second exposure with the shutter closed. Several bias frames are taken each night and then averaged together to get a master bias frame. This master bias frame can then be subtracted from the flat field frames and eventually the image frames. The command *zerocombine* is used to combine the bias frames and the IRAF command *ccdproc* is used to subtract the combined bias frame from flat field frame.

3.1.3 Processing Flat Frames

CCD chips are made up of an array of individual pixels that act as wells for the incoming light. Although these pixels are all similar each will respond a little differently from its neighbor. In order to remove this uneven response distribution, flat field frames are taken. To take a flat field calibration frame, a CCD is exposed to a field where the light is evenly distributed at equal intensities, hence a flat field. If the chip is exposed to an even light field the difference in pixel response can be determined and subtracted from the arc and image frames. Just as the bias frames, the flats are combined into a master flat. This is done using the IFAF command $flatcombine$.

Unlike photometric flats, spectroscopic flats are not taken over the entire CCD. The flat field frames are taken through the spectrograph slit and the even distribution of light is provided by a lamp. Figure 3.4 shows the slit aperture. The result is a small area of the CCD exposed and a sharp drop-off outside of the aperture. There is still some signal outside of the slit caused by noise. If this flat field was subtracted from the image frames, a portion of the object's light would be removed. In order to avoid this, the IRAF command $apflatten$ is used. The task $apflatten$ defines a shape

Figure 3.4: Slit aperture used to take flat field frame

of the slit aperture and removes its effect on the flat frame. The user is prompted to define an aperture for the flat field so that any noise outside that aperture can be set to unity. Figure 3.5 indicates how the aperture was defined in this study. Once an aperture is defined, the master flat must be averaged to create a file called nFlat.imh. The response of the flat can be averaged or fitted to some curve. For this study the master flat was fitted to an order 9, spline3 curve. Fitting the flat field flattens out the spectra of the image frames. This new master flattened frame is then applied to the image frame using the IRAF command *ccdproc*. In order to keep the arc lines well defined, the master flat frame was not applied to the arcs in this study.

3.1.4 Removing Cosmic Rays

Cosmic rays can hit a CCD at anytime during an exposure and registers on the frame as a large spike. These spikes need to be removed before the object frames can be processed. The removal of these cosmic rays is accomplished through the IRAF task *cosmicray*. This task compares the flux of a pixel to its surrounding pixels. If the flux of one pixel exceeds the flux of the average of its surrounding pixels by a threshold value defined by the user, then it is replaced with the average flux of its

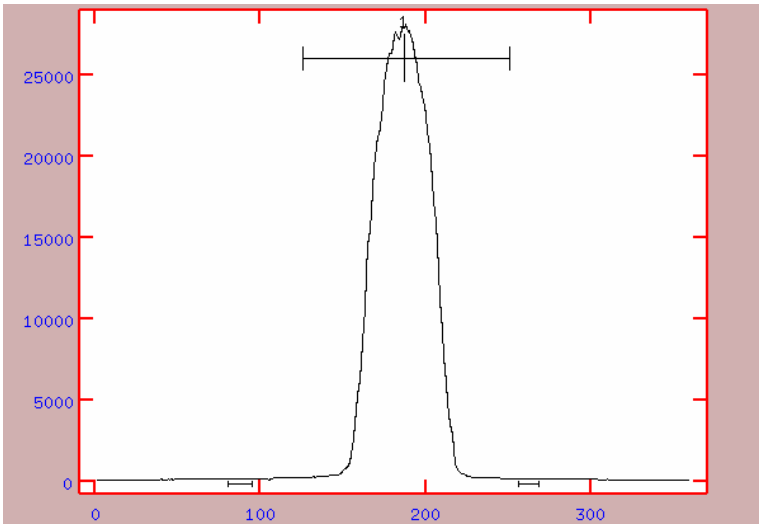

Figure 3.5: Defining the aperture for the flat field. A better signal to noise ratio was found by marking the aperture as shown.

four neighboring pixels. Figure 3.6 shows and example of a specta before and after *cosmicray*. As evident from Figure 3.6, not all the cosmic rays are removed with *cosmicray*. For the best results these events, along with artificial downward spikes caused by imperfections on the CCD, need to be removed manually.

3.1.5 Wavelength Calibration

Images of spectra are graphically represented as the intensity of light over a range of wavelengths. The dispersion of wavelengths across the CCD is recorded as pixel numbers. These spacial relationship of the pixels is not linear with the wavelength of light, therefore it is necessary to preform a calibration to make sure the right pixel is lined up with the appropriate wavelength. This calibration is called a wavelength calibration and is performed in the IRAF package *doslit*. The arc frames are used as the calibration device. An arc frame is a graph of the emission spectra of some gas. In this study iron/argon (FeAr) was used. The emission lines in the spectra have known wavelengths. The arc frames are taken across the same wavelength range as the image frames to ensure a good calibration. Bias- and flat field- corrected image

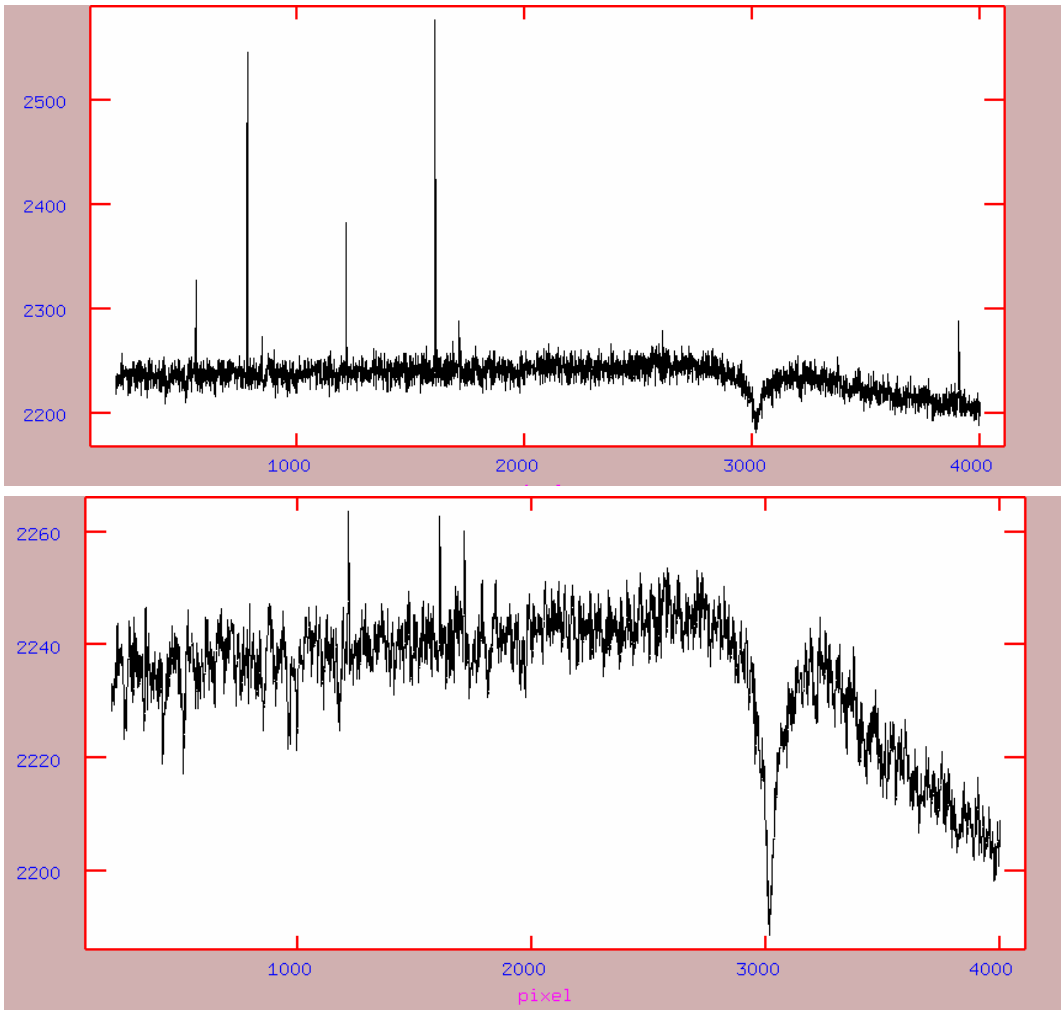

Figure 3.6: A spectrum of AD Arietis before running through *cosmicrays* (*top*). A spectrum of AD Arietis after running through *cosmicrays* (*bottom*).

frames are input into *doslit* where it converts the spectra from two-dimensions into one-dimension for the calibration. Text files must be made to assign the arcs taken on either side of the object, in time, to the object frames they sandwich. These files are called $reftables$ and Figure 3.7 is an example of one used in this study. Just as with the flat frames, an aperture must be defined by the user to wavelength calibrate the object frames. This is necessary for the same reason as the flat field frames. Once the aperture is defined, *doslit* can subtract the noise from the outside of the frames. Spectral lines from the emission spectra must then be marked in order for *doslit* to fit a solution to the arcs. For this study, the FeAr arc frames were taken over a range of 4200 Å to 5000 Å as shown in Figure 3.8. Approximately 20-30 spectral lines were identified and marked, allowing *doslit* to fit a low order dispersion solution. From this solution the object frames can be calibrated to be in terms of wavelength instead of pixels. An object frame from before and after wavelength calibration is shown in Figure 3.9.

```
aicvn0001,aicvn0002,aicvn0003                          arc0011,arc0012
aicvn0004,aicvn0005,aicvn0006,aicvn0007                arc0012,arc0013
aicvn0008,aicvn0009,aicvn0010,aicvn0011                arc0013,arc0014
aicvn0012,aicvn0013,aicvn0014,aicvn0015                arc0015,arc0016
aicvn0016,aicvn0017,aicvn0018,aicvn0019,aicvn0020      arc0016,arc0017
aicvn0021,aicvn0022                                    arc0017
```

Figure 3.7: Example of reftable text.

3.1.6 Continuum Calibration

Continuum calibration fits a low order polynomial function to the curve in the object spectra. Once the fit is found, the spectrum can be flattened for analysis and visual purposes. This is done with the IRAF task *continuum*. This task samples a predetermined amount of points on the spectrum frame and the average of these values is computed. This average is used to determine values that should be rejected,

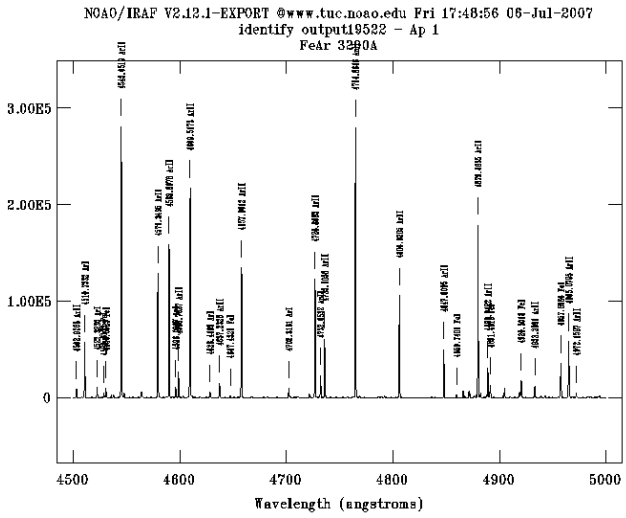

Figure 3.8: FeAr arc map

and then a fitting function is computed. With this function, the continuum of the spectrum is computed. Figure 3.10 shows a spectrum of IQ Virginis before and after continuum calibration.

3.2 Calculating Initial Hydrogen-Beta Values

Initial Hydrogen β color index values were calculated by the IRAF task *sbands* contained under the package *onedspec*. *Sbands* requires three separate text files. The first file is a simple text file of the inputting spectra. Each night is run through *sbands*, inputting the *image.ms.imh* files output from *doslit*. The second text file is a bandpass file that contains information concerning the line being observed and the wide and narrow filters being used. For this research the central wavelength of the Hydrogen β line, at 4861 Å, was used. The filters being used are also input into the bandpass file. If 'none' is placed where the filter would go a square filter is assumed. The width of the filter in Åis also defined in the bandpass file. The third type of text file contains the specifications for the filters, if not square filters. Two filter function

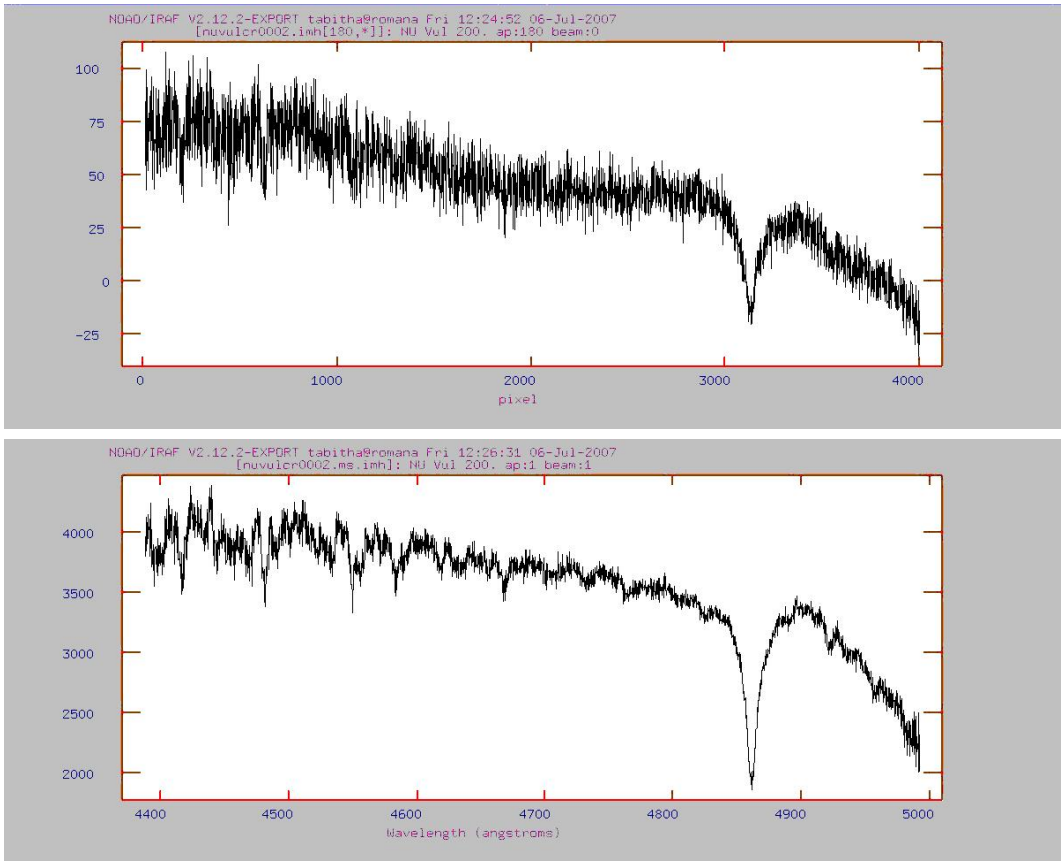

Figure 3.9: A spectrum of NU Vulpeculae before wavelength calibration (*top*). A spectrum of NU Vulpeculae after wavelength calibration (*bottom*).

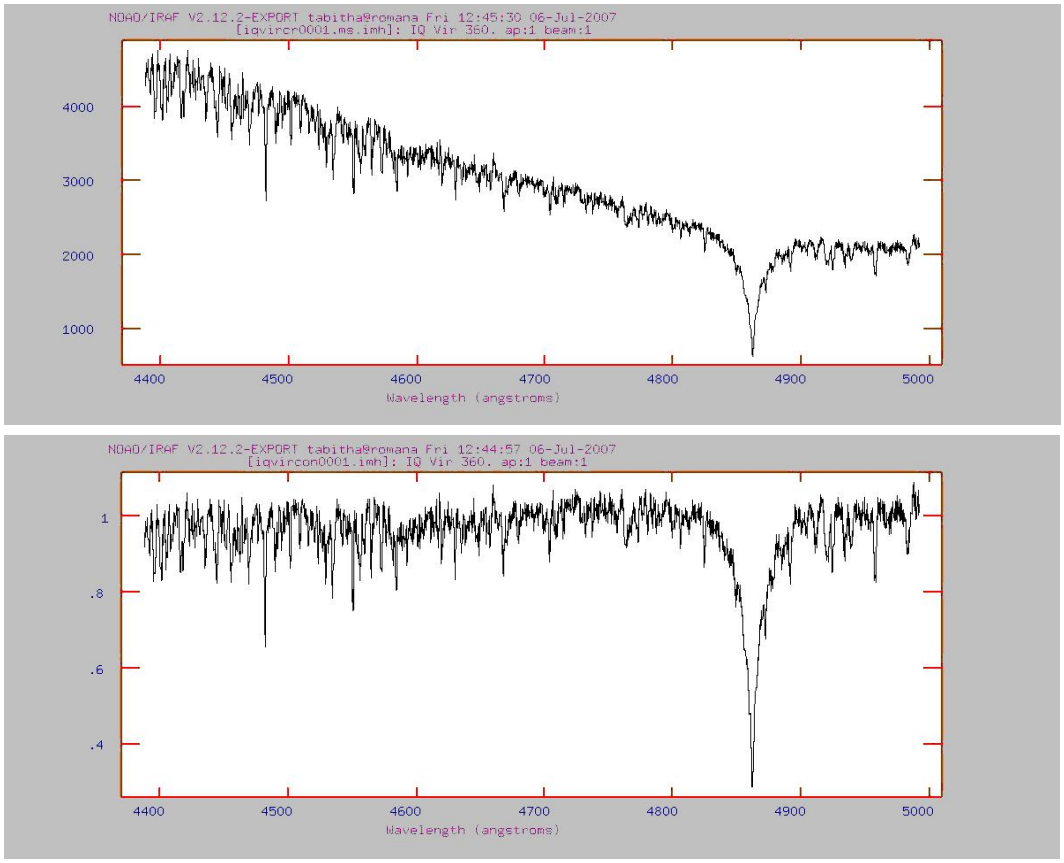

Figure 3.10: A spectrum of IQ Virginis before continuum calibration (*top*). A spectrum of IQ Virginis after continuum calibration (*bottom*).

files are required for single-wavelength color index calculation, a wide filter and a narrow filter. The filter function file is a text file of specific wavelengths and the filter response at that wavelength. Filter functions of Hβ-wide and Hβ-narrow filters from a telescope were modeled to create the filter functions for this project. The graphs of the filter functions were obtained from private communication with Dr. Michael Joner of the Brigham Young University Physics Department.(Joner (2009))

The filter functions modeled where essentially Gaussian curves with a relative response y in Equation 3.1.

$$y = a \exp\left[-(x-b)^2/c^2\right] \tag{3.1}$$

In Equation 3.1, a is the peak height of the Gaussian curve, x is wavelength value, b is the central wavelength of the filter function, and c is given by Equation 3.2.

$$c = FWHM/2\sqrt{\ln(2)} \tag{3.2}$$

For the filter functions, 4861 Å was given as the central wavelength. The relative peak height of the functions were measured by hand. The FWHM value for the Hβ-wide filter is 132 Å. The FWHM value for the Hβ-narrow filter is 28.18 Å. A list of wavelength values was made, in increments of 0.01 Å, and entered into Equation 3.1. This resulted in the list of filter responses needed for the filter function file. *Sbands* was run on these filter functions with a width all the way across the function, referred to as the full width; and a width cut off at the full width half max (FWHM), resulting in a square function with a gaussian top.

Raw Hβ color index values were determined using this method for both the full width gaussian functions and the gaussian functions cut off at the FWHM. This was done for both non continuum calibrated and continuum calibrated frames resulting in four combinations. The raw Hβ index for all four combinations were determined for all the nights in 2002. Tables 3.1 through Table 3.3 give the average values found for each month.

Table 3.1. Average Raw Hβ Color Index Values for March

Star	Full Width Gaussian Filters		FWHM Gaussian Filters		Rodriguez et al. (2000) Hβ
	Cont Hβ	Non-cont Hβ	Cont Hβ	Non-cont Hβ	
AI CVN	1.954	1.944	2.026	2.023	2.707
CQ Lyn	1.982	1.964	2.049	2.040	2.711
CR Lyn	1.950	1.931	2.016	2.006	2.696
DL UMa	1.983	1.964	2.053	2.042	2.731
EN UMa	2.005	1.982	2.077	2.064	2.758
FP Ser	2.061	2.040	2.141	2.129	2.834
HD 120500	2.093	2.071	2.175	2.164	2.871
II Vir	2.029	2.003	2.103	2.088	2.777
κ Boo	2.040	2.026	2.121	2.115	2.806
KW Aur	2.016	2.013	2.096	2.095	2.799
NT Hya	1.967	1.950	2.034	2.024	2.712
PV Gem	1.986	1.969	2.054	2.044	2.731
RX Sex	2.093	2.074	2.174	2.163	2.848
V345 Gem	1.900	1.877	1.958	1.948	2.640
VZ Cnc	1.962	1.959	2.035	2.036	2.709

Table 3.2. Average Raw Hβ Color Index Values for June

Star	Full Width Gaussian Filters		FWHM Gaussian Filters		Rodriguez et al. (2000) Hβ
	Cont Hβ	Non-cont Hβ	Cont Hβ	Non-cont Hβ	
AO Cvn	1.972	1.945	2.069	2.069	2.778
CL Dra	1.993	1.993	2.078	2.065	2.761
CN Boo	1.985	1.954	2.070	2.052	2.771
DK Vir	1.921	1.889	2.003	1.985	2.721
DP Cep	1.967	1.943	2.050	2.036	2.739
DP UMa	1.975	1.942	2.061	2.061	2.770
EI Dra	2.033	2.008	2.143	2.143	2.844
ER Dra	2.005	1.991	2.095	2.085	2.790
FM Com	2.037	2.006	2.129	2.129	2.835
FM Vir	1.957	1.914	2.044	2.044	2.755
γ Boo	1.993	2.816	2.106	2.106	2.816
GG Vir	2.013	1.983	2.102	2.102	2.806
ι Boo	2.033	2.033	2.123	2.101	2.817
IP UMa	1.960	1.934	2.054	2.059	2.783
IQ Vir	2.020	2.020	2.111	2.092	2.823
λ Vir	2.097	2.097	2.193	2.173	2.894
LT Vul	1.959	1.914	2.045	2.045	2.749
ν Vul	1.931	1.931	2.044	2.039	2.791
SAO 141427	1.992	1.992	2.079	2.065	2.767
V1208 Aql	1.987	1.975	2.080	2.090	2.796
V1431 Aql	2.705	2.075	2.206	2.189	2.890
V1438 Aql	1.954	1.916	2.039	2.039	2.726
V1644 Aql	1.880	1.888	2.017	2.021	2.832
V2112 Oph	1.946	1.922	2.031	2.031	2.724
V2314 Oph	1.960	1.938	2.050	2.050	2.775
V383 Vul	1.969	1.942	2.047	2.054	2.741
V544 Lyr	2.012	2.005	2.117	2.117	2.826
V549 Lyr	2.036	2.036	2.128	2.110	2.814
V620 Her	2.012	1.987	2.101	2.101	2.798
V644 Her	1.939	1.924	2.022	2.022	2.709
V831 Her	1.944	1.916	2.026	2.026	2.728
V873 Her	1.954	1.934	2.045	2.045	2.746

Table 3.3. Average Raw Hβ Color Index Values for August

Star	Full Width Gaussian Filters		FWHM Gaussian Filters		Rodriguez et al. (2000) Hβ
	Cont Hβ	Non-cont Hβ	Cont Hβ	Non-cont Hβ	
41 Peg	2.097	2.066	2.208	2.191	2.872
β Cas	1.919	1.888	2.005	1.987	2.721
BH Psc	1.953	1.923	2.029	2.012	2.713
DR Psc	1.926	1.897	2.002	1.986	2.696
EM Aqr	1.963	1.932	2.044	2.028	2.754
ϵ Cep	2.006	1.974	2.079	2.061	2.761
GN And	1.974	1.947	2.057	2.042	2.754
GX Peg	2.030	1.997	2.119	2.101	2.821
HT Peg	2.037	2.004	2.121	2.102	2.836
IK Peg	2.027	2.015	2.111	2.105	2.806
IN Dra	1.944	1.919	2.019	2.005	2.728
LT Vul	1.978	1.948	2.059	2.042	2.749
Sao 107656	1.984	1.953	2.066	2.049	2.774
Sao 52892	2.064	2.034	2.157	2.141	2.834
Sao 72399	2.131	2.101	2.236	2.218	2.888
Sao 88295	2.067	2.057	2.167	2.161	2.895
Sao 143373	1.966	1.936	2.042	2.025	2.743
τ Peg	2.035	2.005	2.122	2.105	2.808
V1208 Aql	2.016	1.982	2.101	2.083	2.796
V1276 Cyg	1.955	1.935	2.037	2.025	2.732
V1438 Aql	1.955	1.931	2.035	2.021	2.726
V1644 Cyg	2.027	2.023	2.120	2.118	2.832
V1719 Aql	1.925	1.900	2.000	1.986	2.710
V2112 Oph	1.950	1.916	2.026	2.007	2.724
V340 And	2.096	2.069	2.195	2.179	2.878
V361 And	1.949	1.922	2.029	2.013	2.717
V388 Cep	1.991	1.961	2.077	2.060	2.734
V396 And	1.949	1.033	2.029	2.019	2.730
V526 Cas	1.997	1.968	2.081	2.065	2.770
V620 Her	2.025	2.011	2.107	2.099	2.798
V831 Her	1.969	1.957	2.040	2.032	2.728
VX Psc	2.049	2.032	2.146	2.147	2.817
VY Psc	1.993	1.968	2.076	2.062	2.777
XX Psc	2.009	1.992	2.097	2.095	2.773

Chapter 4

Analysis and Results

4.1 Analysis of Hydrogen-Beta Values

Linear regressions were run for each observing night in the months of March, June, and August of 2002, for each filter/calibration combination, plotting the Hβ values calculated by *sbands* against the values found in the Rodriguez et al. (2000) catalog. An example of these calibration plots is given in Figure 4.1 from March 06, 2002.

The slopes and correction coefficient for all the calibration plots are given in Table 4.1 through Table 4.3.

The filter/calibration combination of the full width half max filter with a non-continuum-calibrated spectra yielded the best relation, with a slope closest to unity and a high correlation. The calibration equation obtained each night was used to calibrated the raw Hβ values into publishable values. this technique was used for all of the nights with that nights calibration relation for all filter/calibration combinations.

Linear regressions were also calculated for the combination of all observing night in the months of March, June, and August of 2002, making a combined relation for all objects observed within that month. These combined regression relations were done for the filter/calibration combination of the full width half max filter with a non-continuum-calibrated spectra. These combined calibration plots are given in Figure 4.2 for March, June, and August 2002.The slopes and correction coefficient for combined calibration plots are given in Table 4.4. Some data points were removed from the June and August calibration plots due to high errors. The stars removed from the June plot were IP UMa, ν Vul and V1644 Cyg. These stars may have large amplitudes that are throwing the calibration curve off. Two nights, August 14 and 16, were removed entirely from the August plot due to bad flat field calibration frames.

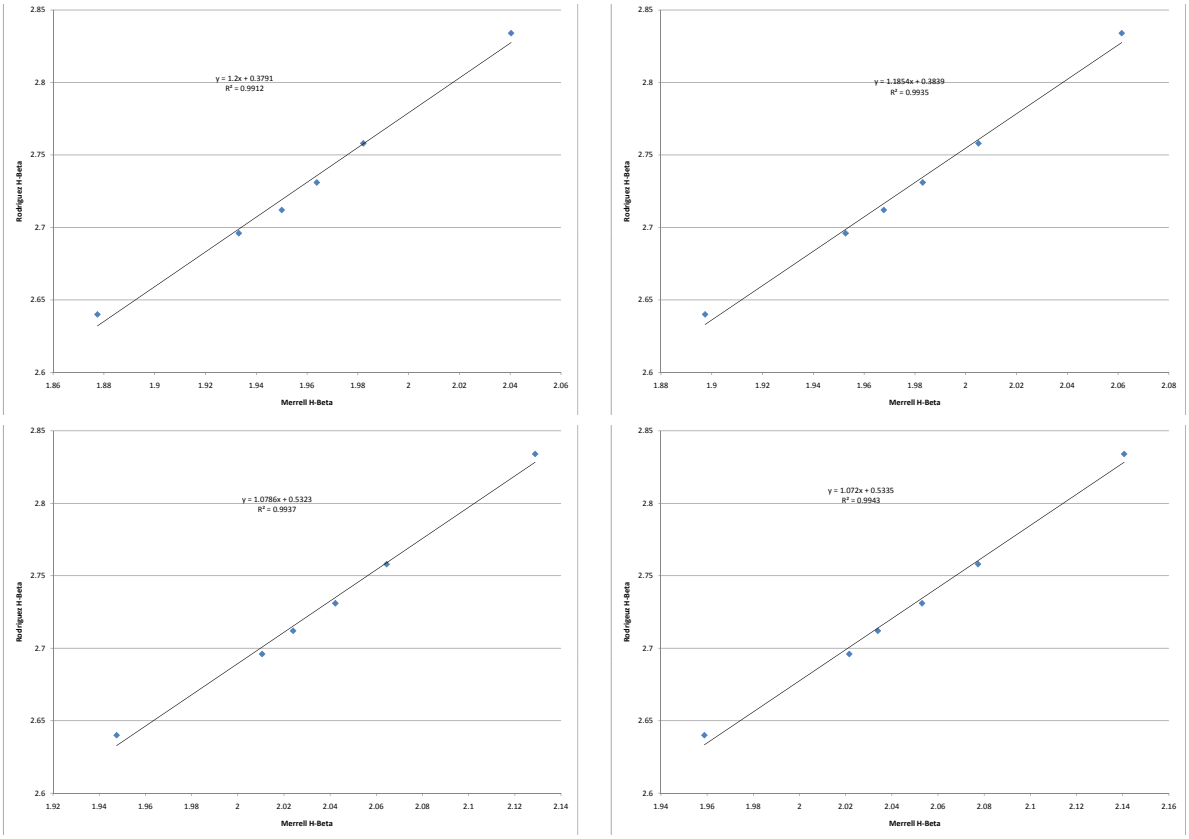

Figure 4.1: Hβ Full Width filter for non-continuum-calibrated spectra on 06 March 2002 (*top-left*),Full Width filter for continuum-calibrated spectra on 06 March 2002 (*top-right*), Full Width Half Max non-continuum-calibrated spectra on 06 March 2002 (*bottom-left*), and Full Width Half Max filter continuum-calibrated spectra on 06 March 2002 (*bottom-right*).

Table 4.1. Relations for Filter/Calibration Combinations for Each Observing Night in March

Gaussian Filter	Calibration	Night	Line Slope	Correlation
Full Width	Non-Continuum	02 Mar	1.339	97%
Full Width	Continuum	02 Mar	1.336	97%
Full Width Half Max	Non-Continuum	02 Mar	1.184	97%
Full Width Half Max	Continuum	02 Mar	1.187	97%
Full Width	Non-Continuum	03 Mar	1.266	98%
Full Width	Continuum	03 Mar	1.224	98%
Full Width Half Max	Non-Continuum	03 Mar	1.117	98%
Full Width Half Max	Continuum	03 Mar	1.098	98%
Full Width	Non-Continuum	04 Mar	1.225	96%
Full Width	Continuum	04 Mar	1.216	98%
Full Width Half Max	Non-Continuum	04 Mar	1.078	98%
Full Width Half Max	Continuum	04 Mar	1.070	98%
Full Width	Non-Continuum	06 Mar	1.200	99%
Full Width	Continuum	06 Mar	1.185	99%
Full Width Half Max	Non-Continuum	06 Mar	1.079	99%
Full Width Half Max	Continuum	06 Mar	1.072	99%

Table 4.2. Relations for Filter/Calibration Combinations for Each Observing Night in June

Gaussian Filter	Calibration	Night	Line Slope	Correlation
Full Width	Non-Continuum	06 Jun	0.736	82%
Full Width	Continuum	06 Jun	0.712	78%
Full Width Half Max	Non-Continuum	06 Jun	0.660	77%
Full Width Half Max	Continuum	06 Jun	0.642	75%
Full Width	Non-Continuum	07 Jun	1.985	93%
Full Width	Continuum	07 Jun	2.055	91%
Full Width Half Max	Non-Continuum	07 Jun	1.287	86%
Full Width Half Max	Continuum	07 Jun	1.287	86%
Full Width	Non-Continuum	08 Jun	1.230	93%
Full Width	Continuum	08 Jun	1.399	93%
Full Width Half Max	Non-Continuum	08 Jun	1.079	97%
Full Width Half Max	Continuum	08 Jun	1.079	97%
Full Width	Non-Continuum	09 Jun	1.020	97%
Full Width	Continuum	09 Jun	0.858	98%
Full Width Half Max	Non-Continuum	09 Jun	0.836	99%
Full Width Half Max	Continuum	09 Jun	0.836	99%
Full Width	Non-Continuum	10 Jun	0.693	91%
Full Width	Continuum	10 Jun	1.142	95%
Full Width Half Max	Non-Continuum	10 Jun	1.036	98%
Full Width Half Max	Continuum	10 Jun	1.036	98%
Full Width	Non-Continuum	11 Jun	0.693	63%
Full Width	Continuum	11 Jun	0.693	62%
Full Width Half Max	Non-Continuum	11 Jun	0.928	81%
Full Width Half Max	Continuum	11 Jun	0.825	78%
Full Width	Non-Continuum	12 Jun	0.462	34%
Full Width	Continuum	12 Jun	0.333	24%
Full Width Half Max	Non-Continuum	12 Jun	0.608	55%
Full Width Half Max	Continuum	12 Jun	0.517	47%

Table 4.3. Relations for Filter/Calibration Combinations for Each Observing Night in August

Gaussian Filter	Calibration	Night	Line Slope	Correlation
Full Width	Non-Continuum	10 Aug	1.654	98%
Full Width	Continuum	10 Aug	1.687	98%
Full Width Half Max	Non-Continuum	10 Aug	1.296	98%
Full Width Half Max	Continuum	10 Aug	1.311	98%
Full Width	Non-Continuum	11 Aug	0.998	86%
Full Width	Continuum	11 Aug	1.049	88%
Full Width Half Max	Non-Continuum	11 Aug	0.952	91%
Full Width Half Max	Continuum	11 Aug	0.969	91%
Full Width	Non-Continuum	12 Aug	1.069	97%
Full Width	Continuum	12 Aug	1.052	97%
Full Width Half Max	Non-Continuum	12 Aug	0.991	98%
Full Width Half Max	Continuum	12 Aug	0.977	98%
Full Width	Non-Continuum	13 Aug	1.189	97%
Full Width	Continuum	13 Aug	1.129	98%
Full Width Half Max	Non-Continuum	13 Aug	1.026	98%
Full Width Half Max	Continuum	13 Aug	0.973	98%
Full Width	Non-Continuum	14 Aug	0.505	63%
Full Width	Continuum	14 Aug	0.499	68%
Full Width Half Max	Non-Continuum	14 Aug	0.500	74%
Full Width Half Max	Continuum	14 Aug	0.541	75%
Full Width	Non-Continuum	15 Aug	1.084	96%
Full Width	Continuum	15 Aug	1.269	97%
Full Width Half Max	Non-Continuum	15 Aug	1.016	98%
Full Width Half Max	Continuum	15 Aug	1.106	98%
Full Width	Non-Continuum	16 Aug	0.920	98%
Full Width	Continuum	16 Aug	1.011	97%
Full Width Half Max	Non-Continuum	16 Aug	1.011	98%
Full Width Half Max	Continuum	16 Aug	0.908	98%

Table 4.4. Combined Calibration Slope and Correlation

Month	Slope	Correlation
March	1.0643	98%
June	0.8703	75%
August	0.08643	93%

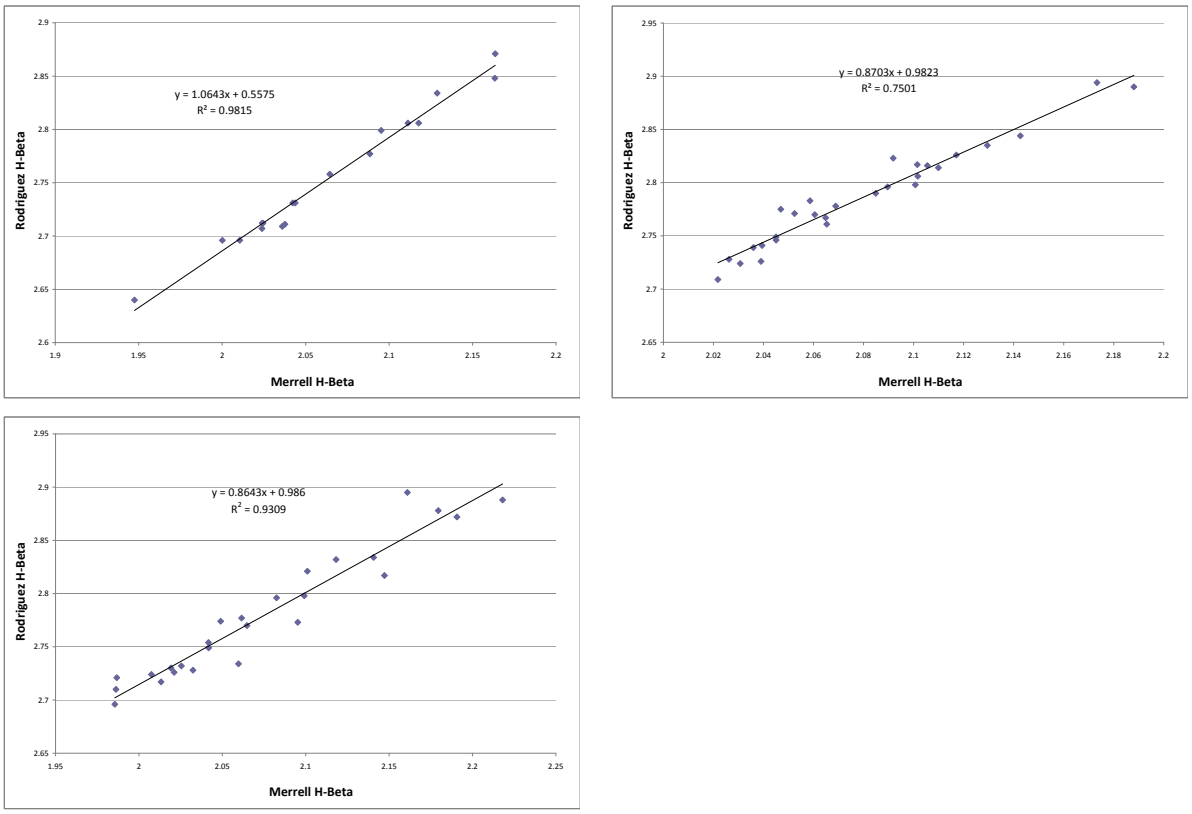

Figure 4.2: Hβ combined calibration relation for March(*top-left*),Hβ combined calibration relation for Jun (*top-right*), Hβ combined calibration relation for August (*bottom-left*).

Table 4.5. Hβ Color Index Values for Stars with No Previously Published Values

Star	Calculated Hβ Values	Raw Hβ Values
CN Dra	2.712±0.013	2.016
CO Lyn	2.699±0.007	2.024
CX UMa	2.797±0.014	2.110
EE Cam	2.718±0.005	2.029
EO UMa	2.730±0.002	2.040
FL Cnc	2.751±0.006	2.067
GG UMa	2.702±0.010	2.015
GW Dra	2.691±0.003	2.006
HQ UMa	2.559±0.304	1.887
NN Peg	2.741±0.003	2.026
QS Gem	2.713±0.003	2.025
V2084 Cyg	2.744±0.013	2.041
V2109 Cyg	2.778±0.008	2.047
V2129 Cyg	2.719±0.040	2.004
V350 Peg	2.724±0.008	2.007
V365 And	2.725±0.012	2.009
V377 Cep	2.735±0.062	2.056
V456 Aur	2.699±0.014	2.009
V830 Her	2.778±0.101	2.012
V919 Her	2.746±0.004	2.048
V929 Her	2.700±0.010	2.001
V966 Her	2.730±0.008	2.032

4.2 Calculating Hydrogen-Beta Values

The Hβ color index values were determined for 18 δ Scuti stars that were unpublished in the Rodriguez et al. (2000) catalog. These values were determined using the calibration fits from the night they were taken. The standard deviations of the results were taken using the standard equation. The color index values and standard deviations are shown in Table 4.5 for the full width half max filter with a non-continuum-calibrated spectra combination. This filter/calibration combination yielded the best results.

The Hydrogen β indices were also determined using the calibration relations from the combined calibration plots for March, June, and August. The results are shown in Table 4.6.

Table 4.6. Hβ Color Index Values for Stars with No Previously Published Values with Combined Calibration

Star	Raw Hβ Values	Hβ Values
CN Dra	2.016	2.747
CO Lyn	2.024	2.712
CX UMa	2.110	2.818
EE Cam	2.029	2.717
EO UMa	2.040	2.729
FL Cnc	2.067	2.758
GG UMa	2.015	2.702
GW Dra	2.006	2.692
HQ UMa	1.887	2.566
NN Peg	2.026	2.755
QS Gem	2.025	2.713
V2084 Cyg	2.041	2.759
V2109 Cyg	2.047	2.769
V2129 Cyg	2.004	2.739
V350 Peg	2.007	2.741
V365 And	2.009	2.742
V377 Cep	2.056	2.776
V456 Aur	2.009	2.696
V830 Her	2.012	2.733
V919 Her	2.048	2.764
V929 Her	2.001	2.723
V966 Her	2.032	2.719

Chapter 5

Conclusions

δ Scuti stars are very interesting stars whose evolution and behavior should continue to be studied. The Hβ color index is a useful way to study them. The Hβ color index of a large collection of spectral data were determined and analyzed in this project. This data was re-reduced with improved techniques in order to improve the Hβ results. The color index was determined for 22 stars with previously unpublished Hβ values.

5.1 Future Projects

There is a lot of information still available from the set of data used in this project. With further analysis of the data publishable Hydrogenβ indices could be determined for at least the 22 stars studied in this project. It was discovered that some of the calibration frames for at least 2 nights in August and possibly one in June were causing large amounts of noise when applied to the object frames for that night. If calibration frames from a different night were applied to the object frames, it is possible to get much cleaner spectra. The calibration relations might also be improved by analyzing the stars used and removing the high amplitude δ Sculti stars.

References

Bush, T. 2007, Master's Thesis, Brigham Young University

Crawford, D. L. 1975, AJ, 80:955-971

Crawford, D. L. 1977, AJ, 83:48-63

Crawford, D. L. 1979, AJ, 84:1858-1865

Crawford, D. L., Mander, J. 1966, AJ, 71:114C

Joner, M. 2009, private communications

Mermilloid, J.C. 1987, Bulletin d'Information du Centre de Donnes Stellaires, 33:44M

Richardson, E.H. 1968, The Royal Astronomical Society of Canada, 62:6

Rodríguez, E., López de Coca, P., Rolland, A., Garrido, R. & Costa, V., 1994, Astron. Astrophys. Suppl. Ser., 106, 21-28

Rodríguez, E., López González, M. J., &López de Coca, P., 2000, A&AS, 144:469-474

Zeilik, M. & Gregory, S. A. 1998, "Introductory Astronomy & Astrophysics" (Saunders College Publishing)